Applied Catalysis B: Environmental 180 (2016) 6–12

Contents lists available at ScienceDirect

Applied Catalysis B: Environmental

journal homepage: www.elsevier.com/locate/apcatb

Valence state heterojunction $Mn_3O_4/MnCO_3$: Photo and thermal synergistic catalyst

Gang Wang[a], Baibiao Huang[a,*], Zaizhu Lou[a], Zeyan Wang[a], Xiaoyan Qin[a], Xiaoyang Zhang[a], Ying Dai[b,**]

[a] State Key Laboratory of Crystal Materials, Shandong University, Jinan 250100, People's Republic of China
[b] School of Physics, Shandong University, Jinan 250100, People's Republic of China

ARTICLE INFO

Article history:
Received 27 April 2015
Received in revised form 2 June 2015
Accepted 5 June 2015
Available online 9 June 2015

Keywords:
Valence state heterojunction
$Mn_3O_4/MnCO_3$ composites
Photo and thermal synergistic catalysis

ABSTRACT

The valence state $Mn_3O_4/MnCO_3$ heterojunctions were synthesized using a facile, wet chemical oxidation method during hydrothermal process. Their crystal structures, morphologies and optical properties were systematically investigated. The obtained $Mn_3O_4/MnCO_3$ exhibited photo and thermal synergistic catalysis which have been estimated via degradation of methylene blue (MB) and HCHO under visible light ($\lambda > 420$ nm) irradiation at different temperature (20 °C, 60 °C and 80 °C). Mn_3O_4 and $MnCO_3$ possessed matching band potentials that could prevent the recombination rate of photogenerated electrons and holes in the reaction, which proved by the PL intensity of the samples, resulting in a great enhancement on their catalytic efficiency. Catalytic activity of $Mn_3O_4/MnCO_3$ under photo and thermal effect was not the simple summation of photocatalysis and thermocatalysis, but a synergistic effect was existed in $Mn_3O_4/MnCO_3$ composites which possessed much lattice oxygen to capture the holes leading to efficiently oxidizing reaction at high temperature. A possible mechanism was proposed based on valence state heterojunction to illustrate the synergistic effect between photo and thermal catalysis on degradation of organic pollutions.

1. Introduction

Development of modern human being society is based on the continuous expending fossil energy, causing pollution of environment including water, air and soil. Especially for water pollution, thousands of organic compounds which are frequently toxic and non-biodegradable threat the survival of mankind. In recent years, the materials which have applications in pollution treatment have attracted more attentions. In various materials for pollution treatment, multivalence compounds have a unique advantage in the degradation of pollutants in water and air. Many works have reported the removal of pollutions using iron/carboxylate oxidation systems, which contain oxalic, citric and tartaric acids, to improve the degradation of contaminants such as dyes, formaldehyde, and benzene [1–3]. Elements with multivalence states can facilely transfer energy by the interchangeable between different valence states, which always happen in multitudinous catalytic reactions, including photocatalytic reactions [4]. Recently, our group found a new valence state heterojunctions photocatalyst CuO/CuSCN [4], which coupled with two different cupreous valance states compounds, and then form the heterojunction composites. Due to the transfer of electron between Cu(I) and Cu(II), the recombination of photo-carriers was efficient limited resulting in enhanced photocatalytic activity. Therefore, multivalence compounds are potential strategy to explore high efficient photocatalysts.

Similar with copper, manganese also has varieties of valence states (+2, +3, +4, +6, +7) which are rich in reserves on the earth and interchangeable under mild conditions. As we known, biochemical function of all life on our earth is interrelated with the valence change of manganese, especially in photosynthesis [5]. Bonchio et al. found the functional core of oxygenic photosynthesis was in charge of catalytic water oxidation by a multi-redox Mn^{III}/Mn^{IV} manifold which is the expected turning point for artificial photosynthesis [5,6].

Many works have reported that manganese compounds are excellent thermalcatalytic materials for oxidation of HCHO and CO in high temperature [7–10]. Alvarez et al. [8] reported that Mn/Al_2O_3 and $Mn\text{-}Pd/Al_2O_3$ could oxide HCHO under 220 °C and 90 °C, respectively. Temperature is a crucial factor in traditional

* Corresponding author. Fax: +86 531 8836 5969.
** Corresponding author. Fax: +86 531 8836 5569.
E-mail addresses: bbhuang@sdu.edu.cn (B. Huang), daiy60@sdu.edu.cn (Y. Dai).

http://dx.doi.org/10.1016/j.apcatb.2015.06.010
0926-3373/

catalytic reactions, the higher temperature always leads to higher catalytic efficiency. Some reports have verified that temperature also enhance the photocatalytic reaction by fasting surface reactions. Datye and Kennedy reported catalytic oxidation of ethanol reaction over TiO_2 and Pt/TiO_2, which exhibited significant photo and thermal synergistic effect [11]. Owing to the abundant photothermal energy around the world, the combination of light and heat would greatly raise the utilization rate of solar energy. However, the detailed mechanism of thermal enhanced photocatalytic reaction was still unclear and need to do more work. Most of Mn compounds have excellent capacity for harvesting visible light. And, a major portion of researches reported Mn as one of visible light sensitized elements in photocatalysis field [12–15]. So, mixed-valent manganic compound will be potential materials which have photo and thermal synergistic effect on catalytic efficiency

Herein, we design a valence state heterojunction composites $Mn_3O_4/MnCO_3$, which was facile obtained via one step hydrothermal method with the addition of H_2O_2. Mn_3O_4 greatly enhanced the visible light absorption of $Mn_3O_4/MnCO_3$ composites which exhibited excellent photo and thermal synergistic effect on degradation of methylene blue and HCHO at high temperature. The band structure of Mn_3O_4 and $MnCO_3$ could form heterojunction of type II that can greatly decrease the recombination rate of photoinduced carries which have been verified by their photoluminescence spectra. The photo and thermal synergistic catalytic effect was attributed to the lattice oxygen in $Mn_3O_4/MnCO_3$ composites which could capture the photogenerated holes for oxidizing MB or HCHO, and quickly migrate at high temperature. The detailed mechanism was proposed to illustrate photo and thermal synergistic effect on degradation of MB and HCHO.

2. Experiment

2.1. Synthesis

$Mn_3O_4/MnCO_3$ composites were synthesized via hydrothermal method, in a typical synthetic route, 0.01 mol $Mn(CH_3COO)_2$ and 0.02 Na_2CO_3 were mixed in 80 ml deionized water for stirring 6 h, and then a certain amount of H_2O_2 (30%) was introduce as oxidant to generated Mn^{3+} to form Mn_3O_4. After one hour stirring, the mixed suspensions transferred to 120 ml sealed teflon-lined auto-clave and followed by hydrothermal treatment at 100 °C for 12 h. The sample was collected by filtration, and then thoroughly washed with deionized water and ethanol, and finally vacuum drying in an oven at 40 °C overnight. The pure $MnCO_3$ was obtained by using 0.01 mol $Mn(CH_3COO)_2$, 0.01 Na_2CO_3 as raw materials and without adding of H_2O_2 in the same hydrothermal condition.

2.2. Characterization of the samples

The X-ray powder diffraction (XRD) patterns of the as-prepared products were characterized by using a Bruker AXS D8 advance powder diffractometer (Cu Kα X-ray radiation, λ = 0.154056 nm). X–ray photoelectron spectroscopy (XPS) measurements were performed on a Thermo Fisher Scientific Escalab 250 spectrometer with monochromatized Al Kα excitation, and C1s (284.6 eV) was used to calibrate the peak positions of the elements. Scanning electron microscopy (SEM, Hitachi S-4800 microscope) and high-resolution transmission electron microscopy (HRTEM, JEOL JEM-2100, 200 kV) were employed to observe the morphologies and micro-structures. A Builder 4200 instrument was used to measure the Brunauer- Emmett-Teller (BET) surface areas of the samples at liquid nitrogen temperature. The photoluminescence (PL) measurements of the samples were carried out on a Hitachi F-4500 fluorescence spectrophotometer at room temperature (the excited wavelength was 248 nm). UV–vis diffuse reflectance spectra were obtained for the dry-pressed disk samples by using a Shimadzu UV 2550 recording spectrophotometer, which was fitted with an integrating sphere, and $BaSO_4$ was used as a reference.

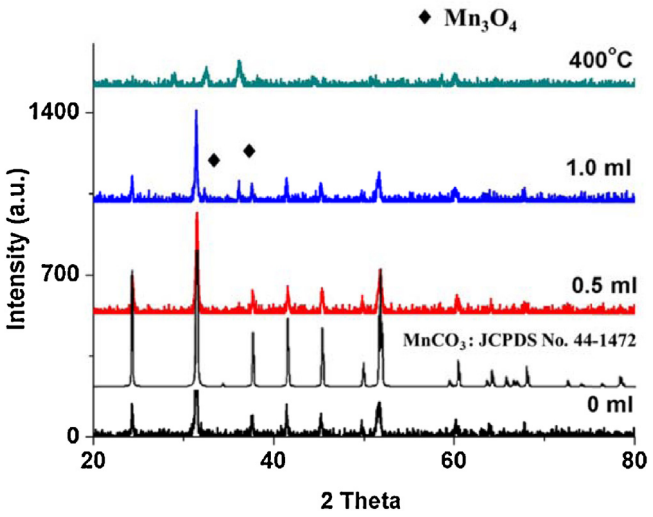

Fig. 1. XRD results of different samples, 0 ml, 0.5 ml, and 1 ml are the amount of H_2O_2 during synthesized process, and the green one is Mn_3O_4 which is obtained by calcining ready-made $MnCO_3$ under 400 °C for 5 h. The standard XRD of $MnCO_3$ is also displayed.

2.3. Photocatalytic reaction

The photocatalytic performance of the as-prepared samples was characterized by decomposing methylene blue (MB) and HCHO under visible light irradiation at a given temperature. A 300 W Xe arc lamp (PLS-SXE300, Beijing Trusttech Co., Ltd.) equipped with an ultraviolet cutoff filter to provide visible light (λ > 420 nm) was used as the light source, and the distance between the liquid surface of the suspension and the light source was set about 15 cm. The photodegradation experiments were carried out with the sample powder (100 mg in MB solution and 300 mg in HCHO solution) suspended in MB aqueous solution (100 ml, 20 mg l^{-1}) or HCHO solution (300 ml, 1.5 M) with constant stirring. Prior to irradiation, the suspensions were magnetically stirred in the dark for 1 h to establish adsorption/desorption equilibrium. At the given time intervals, about 5 ml of the MB suspension was taken for further analysis after centrifugation. MB photodegradation were analyzed at 664 nm as a function of irradiation time on a UV–vis spectrophotometer (TU-1810, Pgeneral, Beijing). Photoacoustic Field Gas-Monitor (INNOVA 1412) was used to measure the concentration of CO_2 during the degradation of HCHO. We used the heating jacket to keep the temperature at 20, 60, 80 °C, respectively, in three-neck flask. In order to avoid evaporation, the necks of flask were sealed.

3. Results and discussion

3.1. XRD, SEM, TEM and XPS

Fig. 1 is the XRD pattern of $MnCO_3$, Mn_3O_4 and $Mn_3O_4/MnCO_3$ samples. It is observed that all the peaks of pure $MnCO_3$ coincide with the standard rhombohedral $MnCO_3$ phase (JCPDS No. 44-1472), and no other peak is found. As the amount of H_2O_2 increased to 1 ml, the peaks of tetragonal Mn_3O_4 (JCPDS No. 24-734) could be observed clearly, which indicated Mn_3O_4 could be integrated in our system. When the amount of H_2O_2 was not sufficient, we could not observe the peak of Mn_3O_4 by XRD measurement (red). The pure

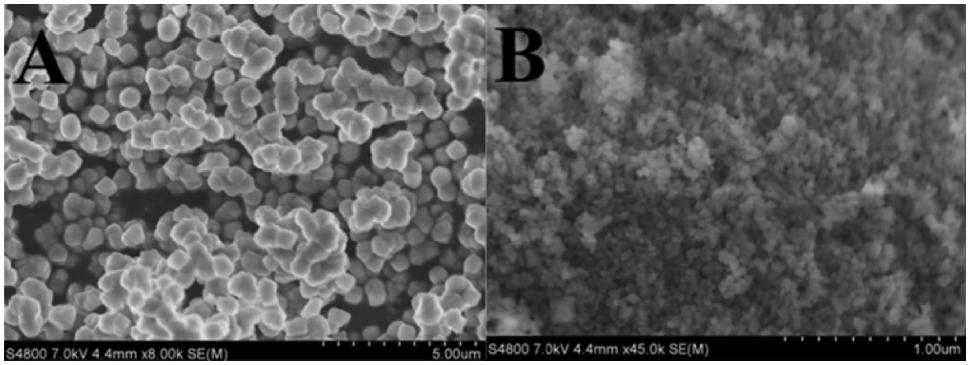

Fig. 2. SEM images of pure $MnCO_3$ (A), and $Mn_3O_4/MnCO_3$ (B) ($Mn_3O_4/MnCO_3$ with 1.0 ml H_2O_2).

Mn_3O_4 was obtained by calcining purchased $MnCO_3$ in 400 °C for 5 h.

The morphologies of the as-prepared products were characterized by SEM, which are shown in Fig. 2. As shown in Fig. 2A and a, the pure $MnCO_3$ were spherelike particles with relatively uniform size, range from 500 nm to 700 nm. When H_2O_2 was introduced to the reaction, nanosized particles were obtained. Fig. 2B and b displays the morphology of $Mn_3O_4/MnCO_3$ composites, which were small cubic with the size of 50 nm. Suib et al. reported that H_2O_2 played an important role in adjusting crystal growth and controlling particle size of manganese oxide. During the synthesis of manganese oxide, H_2O_2 could increase the reaction rate of forming manganese oxide, which will accelerate the crystallization process and limit the particle growth speed, and then narrow the particle size [16]. Due to more active sites, small particles benefit for photocatalytic activity. The size of $Mn_3O_4/MnCO_3$ composites which prepared with 0.5 ml H_2O_2 was about 100 nm. When H_2O_2 increased to 1.5 ml, the morphology was basically the same as that with 1.0 ml (Fig. S1 Supporting information). The structure of the $Mn_3O_4/MnCO_3$ composite was further studied by TEM and HRTEM. Fig. 3A shows the typical TEM image of $Mn_3O_4/MnCO_3$ (1 ml H_2O_2). The HRTEM image of the magnified view of the sample is given in Fig. 3B. As can be seen, two sets of different fringes are found. The lattice fringe of 0.496 nm corresponds to the (1 0 1) crystal plane of Mn_3O_4, while the fringe of 0.352 nm matches well with the (0 1 2) plane of $MnCO_3$.

To further determine the valance state of the $Mn_3O_4/MnCO_3$ composites, XPS measurements were employed to analyze. Fig. 4c is the full XPS survey scan of $Mn_3O_4/MnCO_3$ composites which exhibit the characteristic peaks of C 1s, Mn 3d and O 1s. From the high resolution XPS patterns of Mn 2p and O 1s in Fig. 4a and b, it is observe that both binding energy of Mn $2p_{3/2}$ and Mn $2p_{1/2}$ can be described as the superposition of two peaks by a Gaussian distribution. According to the literature, the located binding energies around 639.6 eV, 651.4 eV and 642.1 eV, 653.3 eV are attributed to Mn^{II} $2p_{3/2}$, $2p_{1/2}$ and Mn^{III} $2p_{3/2}$, $2p_{1/2}$, respectively [17–19]. According to the XPS results of $Mn_3O_4/MnCO_3$ composites that obtained with 0.5, 1.0, and 1.5 ml H_2O_2, the molar ratio of $MnCO_3$ and Mn_3O_4 were about 6.69:1, 1.8:1 and 2.05:1 (Figs. 4 and S3 (Supporting information)), respectively. $Mn_3O_4/MnCO_3$ composites prepared with 1.0 ml H_2O_2 possessed highest catalytic activities under visible light irradiation at 80 °C (Fig S2, Supporting information), which molar ratio of $MnCO_3$ and Mn_3O_4 was 1.8:1. Therefore, the following experiments were characterized over this sample. The satellite feature of Mn^{II} is around 646 eV. Fig. 4B is the high resolution results of O 1s which indicate three peaks by a Gaussian distribution, locate around 530.9 eV, 531.8 eV, and 532.6 eV, respectively. The O 1s peak at 531.8 eV is assigned to oxygen in CO_3^{2-} [20]. The low binding energy component located at 530.9 eV is attributed to the lattice oxygen in Mn_3O_4 [21–23]. The additional binding energy component, centered at 532.6 eV is associated with OH group [24]. These results confirmed that Mn_3O_4 had successfully combined with $MnCO_3$ crystals, and amount of lattice oxygen was also in $Mn_3O_4/MnCO_3$ structure. The lattice oxygen in $Mn_3O_4/MnCO_3$ was the main reason for photo and thermal synergistic effect on degradation of MB and HCHO molecules which will be discussed in mechanism part in detail.

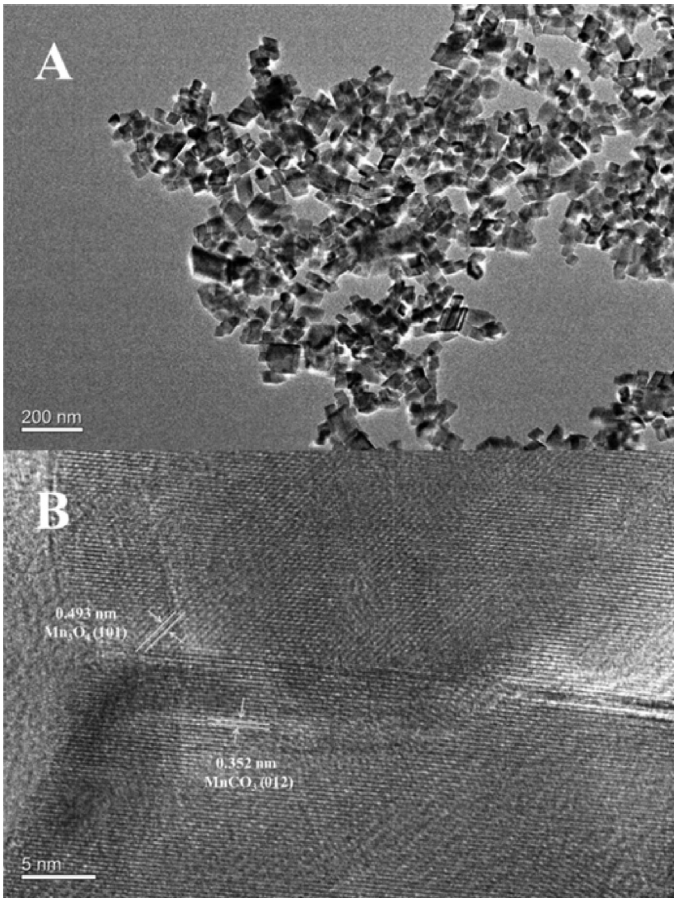

Fig. 3. A is the TEM image of $Mn_3O_4/MnCO_3$ composites (1 ml H_2O_2), and B is the HRTEM of corresponding magnified view of the interface between Mn_3O_4 and $MnCO_3$.

3.2. Optical absorption properties.

Fig. 5A is the UV–vis diffuse reflectance spectra of the samples. As can be seen below, pure $MnCO_3$ has an absorption edge at about 250 nm which only absorb ultraviolet light, while $Mn_3O_4/MnCO_3$ possesses a broader absorption in the whole visible light region.

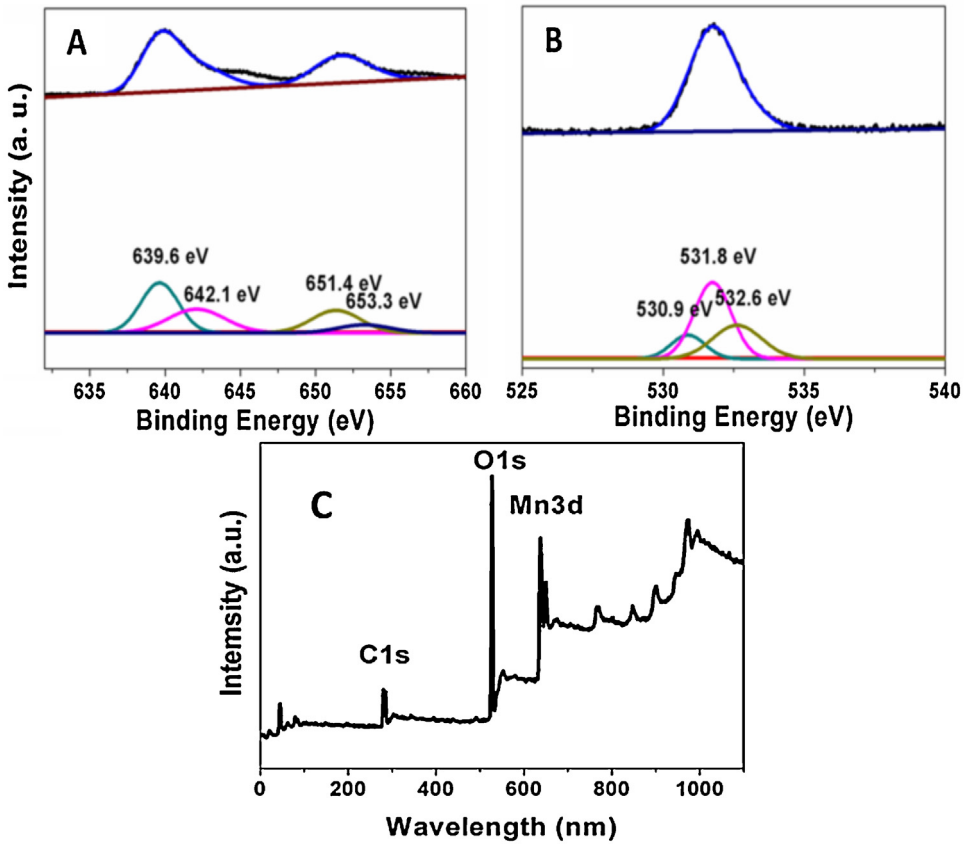

Fig. 4. The high resolution XPS spectroscopic spectra of Mn 2p and O 1s in $Mn_3O_4/MnCO_3$ (A and B), C is the full XPS survey scan of $Mn_3O_4/MnCO_3$ composites.

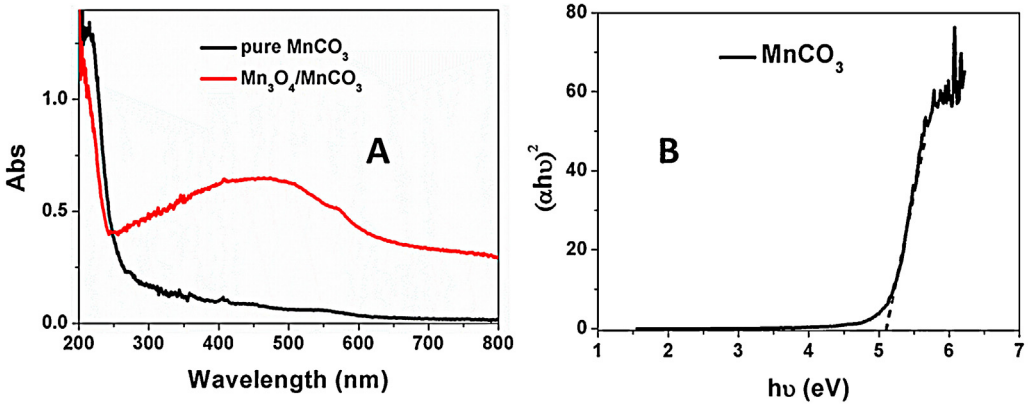

Fig. 5. A, UV–vis diffuse reflectance spectra of pure $MnCO_3$ and $Mn_3O_4/MnCO_3$ (1 ml, H_2O_2). B, Plots of $(\alpha h\nu)^2$ versus energy $h\nu$ of the pure $MnCO_3$ band gap.

The component of Mn_3O_4 greatly enhanced the visible light absorption of $Mn_3O_4/MnCO_3$ composites, which is capable of responding under visible light irradiation. We have known that Mn_3O_4 is a p-type semiconductor with a wide direct bandgap of 2.3 eV [25–27]. In order to confirm the bandgap of $MnCO_3$ semiconductor, the equation is needed below: [28,29]

$$\alpha h\nu = A(h\nu - E_g)^{\frac{n}{2}}$$

In the equation, α, ν, E_gE_g, and$A$ represent absorption coefficient, light frequency, band gap, and a constant, respectively. "n" is a certain number which determined by the optical transition type of semiconductor. When the semiconductor is direct transition type n is 1, and 4 for an indirect transition. $MnCO_3$ is a kind of direct transition type semiconductor, n is 1. Fig. 5B is the band gap energy of $MnCO_3$, which is determined from a plot of $(\alpha h\nu)^2$ vs $(h\nu)$ and is about 5.0 eV.

Band structure of $MnCO_3$ and Mn_3O_4

There is no literature reported on the band structure of bulk $MnCO_3$ and Mn_3O_4, we must estimate the VB and CB of $MnCO_3$ and Mn_3O_4 by the equation below [30–32]:

$$E^0_{CB} \approx E_{CB} \approx \chi_{comp} - E^e - \frac{1}{2}E_g$$

The equation is based on the reasonable assumption that the pH value of the solution at the zero point of charge. E^0_{CB} is the CB edge of a semiconductor at the zero charge, which equals approximately to E_{CB}. χ_{comp} is electronegativity of a compound which is given by the geometric mean of the electronegativities of the constituent

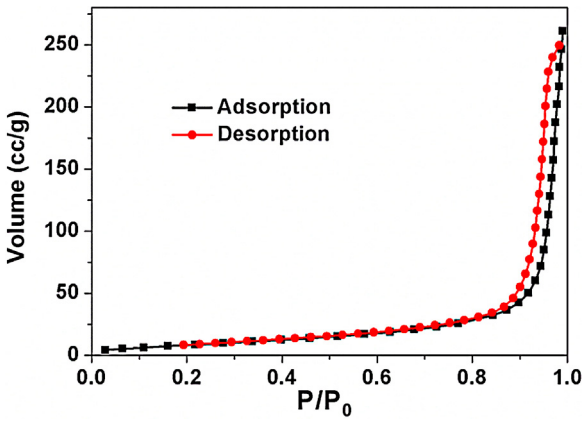

Fig. 6. Typical nitrogen adsorption-desorption isotherm of $Mn_3O_4/MnCO_3$ (obtained with 1.0 ml H_2O_2).

atoms [31]. E^e and E_g are the energy of free electrons and the band gap of the semiconductor, respectively, on the hydrogen scale, and $E^e \approx 4.5eV$. Therefore, we obtain the CB edge of $MnCO_3$ is estimated to be −0.27 eV and 5.27 eV with respect to NHE (normal hydrogen electrode). To Mn_3O_4, the CB edge is approximately −0.41 eV and CB is 1.89 eV (NHE).

3.2.1. BET

Surface area is an important factor of influencing the photocatalytic activity. The higher surface area possesses more activity sites, which benefit photocatalytic reaction. The BET surface area of $Mn_3O_4/MnCO_3$ composites was carried out at liquid nitrogen temperature, and Fig. 6 is the plot of nitrogen adsorption-desorption isotherm which can be classified to a type-IV isotherm. The BET specific surface area of $Mn_3O_4/MnCO_3$ was 33.5 m^2/g and pure $MnCO_3$ was about 7.9 m^2/g.

3.3. Photocatalytic Activities

The photocatalytic activities of $Mn_3O_4/MnCO_3$ (obtained with 1.0 ml H_2O_2) were measured by decomposing methylene blue (MB) and HCHO under visible light irradiation at different temperature. Fig. 7A is the degradation of MB dye under visible light irradiation (λ > 420 nm) at different temperature (20, 60 and 80 °C), which show great difference as the temperature increasing. In the case of 60 °C, about 62% MB dye could be decomposed over $Mn_3O_4/MnCO_3$ after 3 h reactions, and about 88.7% MB dye could be degraded at 80 °C after the same time reaction. There was almost no degradation efficiency over MB at 20 °C except the self-decomposed of MB under light irradiation. The blank and contrast experiments were presented in Fig. 7B. The black column in Fig. 7B is the adsorption process at different temperature (20, 60, and 80 °C) without light irradiation for 3 h stirring and the results displayed the high temperature could not decompose MB dye in the dark. The red column in Fig. 7B is the self-degradation of MB dye, which was obtained without samples under visible light irradiation for 3 h. We could not find obviously decomposed of MB dye after 3 h stirring at 20, 60, or 80 °C, and the self-degradation efficiency of MB was independent of temperature. The blue column was the degradation efficiency of $Mn_3O_4/MnCO_3$ composites under visible light irradiation at different temperature for 3 h. Therefore, the catalytic process of $Mn_3O_4/MnCO_3$ composites exhibited obviously photo and thermal synergistic effect on degradation of MB dye, and the reactions were repressed without light irradiation at different temperature. The catalytic activities of original-Mn_3O_4 or original-$MnCO_3$ were also performed in Fig. S2 A and B (Supporting information).

To our knowledge, manganese compounds may have excellent thermal catalytic efficiency on degradation of formaldehyde. Fig. 7C is photo and thermal synergistic effect for decomposing of HCHO molecules in solution at different temperature. During the reactions, the concentration of CO_2 did not change at 20 °C under visible light irradiation. When the temperature was raised to 60 °C, the

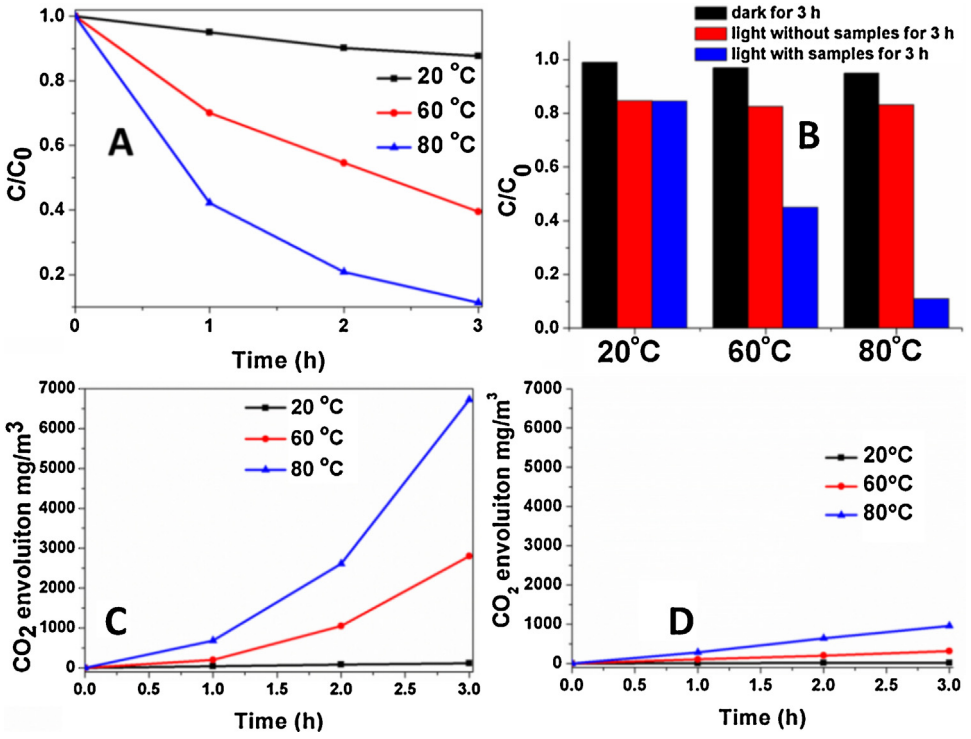

Fig. 7. Photodegradation of MB dye and HCHO solutions at different temperature as a function of irradiation time over $Mn_3O_4/MnCO_3$. (A) Illuminating and heating process of degradation of MB at 20, 60, 80 °C. (B) Heat in dark (black), light without samples (red) and light with samples (blue) in MB solution at different temperature (C) Illuminating and heating process of degradation of HCHO at 20, 60, 80 °C. (D) Thermocatalysis of $Mn_3O_4/MnCO_3$ at different temperature.

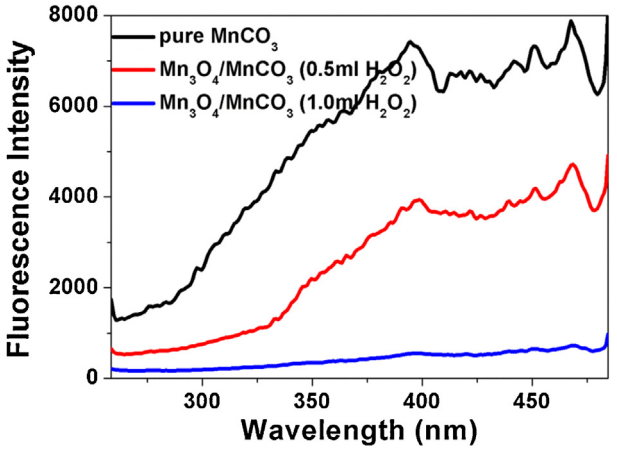

Fig. 8. PL spectra of the $MnCO_3$, $Mn_3O_4/MnCO_3$ obtained with 0.5 ml and 1.0 ml H_2O_2. (λ_{ecx} = 248 nm).

concentration of CO_2 distinctly increased as time change, which implied the HCHO molecules have been decomposed. The greater concentration of CO_2 was emerged if the temperature was further raised to 80 °C. HCHO molecules could be more efficiently decomposed at higher temperature. The comparison thermocatalysis of $Mn_3O_4/MnCO_3$ is shown in Fig. 7D. The concentrations of CO_2 slowly increased at the temperature of 60 °C and 80 °C. Although the thermocatalysis of $Mn_3O_4/MnCO_3$ led to a certain degradation efficiency of HCHO at higher temperature, the effect was unattractive when compared to that of photo and thermal synergistic results. The decomposed efficiency could be significantly enhanced by the combination of thermal and light irradiation. Therefore, $Mn_3O_4/MnCO_3$ composites displayed obviously photo and thermal synergistic effect on degradation of MB and HCHO. The photocatalytic experiments proved superoxide anion, photo-generated hole and •OH radical were all not main active species in photo and thermal catalytic process. Therefore, the photo-generated holes could be capture by the lattice oxygen in Mn_3O_4 to form the sole active specie, and then degrading MB and HCHO (see Fig. S4 Supporting information).

3.4. PL spectra

The amount of photo-generated electrons and holes is largely affected the efficiency of photocatalytic reactions. The recombination of photoinduced carriers will reduce the quantum yield. The photo-luminescence emission spectra can directly detect the recombination ratio of the free carriers which is an appropriate method for understanding the separation capacity of the heterojunction semiconductor composites [33,34]. The intensity of PL spectra can directly reflect the amounts of carriers which participate in the photocatalytic process, the low PL intensity implies the recombination rate of photogenerated carriers is repressed. Fig. 8 is the PL spectra of different samples, with the excitation wavelength at 248 nm. It can observed that pure $MnCO_3$ shown a strong emission at visible light region, which was originating from direct recombination of electrons and holes. $Mn_3O_4/MnCO_3$ heterojunction composites exhibited relatively lower PL intensity which meant the photo-generated carriers could easily transfer at the interface between Mn_3O_4 and $MnCO_3$. Thereby, the recombination rate of photo-carriers had been restrained.

3.5. Possible photocatalytic mechanism

As is known, photoinduced electrons and holes easily recombine on the surface of semiconductors. So the photocatalytic efficiency

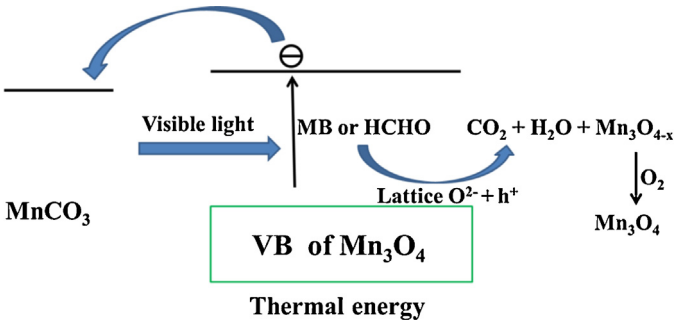

Fig. 9. The scheme diagram of possible reaction mechanism of photo and thermal synergistic effect.

of materials greatly depends on the photogenerated carrier lifetime [35]. The photocatalytic activity is closed related to the band structure of semiconductor. Fig. 9 shows the schematic diagram of Mn_3O_4 and $MnCO_3$ band structure, which was based on the band position calculation above. It is observed that the band structures of Mn_3O_4 and $MnCO_3$ have a matching band position. Due to the CB potential of Mn_3O_4 is negative than that of $MnCO_3$, the photogenerated electron could transfer to $MnCO_3$ CB through the interface between Mn_3O_4 and $MnCO_3$. This property prevents the recombination of electrons and holes, which prolong the lifetime of photo-carriers. Holes in VB of Mn_3O_4 have ample time to be captured by lattice oxygen in Mn_3O_4 that is greatly important to photo and thermal synergistic catalytic effect.

The thermocatalysis effects of metal oxides follow the law of Mars-van Krevelen oxidation-reduction [36,37]. Fig. 9 shows the photo and thermal synergistic effect mechanism of $Mn_3O_4/MnCO_3$. Mn_3O_4 semiconductor was excited by visible light to produce electrons and holes. The electrons transferred to the CB of $MnCO_3$, which created conditions for holes to be captured by lattice oxygen in Mn_3O_4. The Mn_3O_{4-x} formed after lattice oxygen oxidizing MB or HCHO, then restored to Mn_3O_4 owing to the existence of O_2 in the solution. The electric conductivity of lattice oxygen can be increased as the temperature rising, which cause more holes transfer to the surface and participate in catalytic process [38].

4. Conclusion

Valence state heterojunction $Mn_3O_4/MnCO_3$ have been fabricated via H_2O_2 oxidation in hydrothermal process. $Mn_3O_4/MnCO_3$ composites exhibited enhanced visible light absorption, and displayed photo and thermal synergistic effect on degradation of methylene blue and formaldehyde. PL intensity of $Mn_3O_4/MnCO_3$ composites was greatly decreased due to the lower recombination of photogenerated carriers in suitable semiconductor structure. The photogenerated electron could transfer to $MnCO_3$ CB through the interface between Mn_3O_4 and $MnCO_3$ which prolong the lifetime of holes. Lattice oxygen in Mn_3O_4 played an important role in photo and thermal synergistic oxidation process, which capture the photoinduced holes and move quickly due to the enhanced electric conductivity of lattice oxygen in high temperature. The experiments show that $Mn_3O_4/MnCO_3$ valence state heterojunction were efficient under interaction of photo and thermal. This work extends the scope of the photocatalytic materials and may have more potential applications in environment.

Acknowledgements

This work was financially supported by research grants from the National Basic Research Program of China (the 973 Program; No.

2013CB632401), the National Natural Science Foundation of China (Nos. 21333006, 51321091 and 11374190).

Appendix A. Supplementary data

Supplementary data associated with this article can be found, in the online version, at http://dx.doi.org/10.1016/j.apcatb.2015.06.010

References

[1] E. Rodriguez, G. Fernandez, B. Ledesma, P. Alvarez, F.J. Beltran, Appl. Catal. B 92 (2009) 240–249.
[2] Y.H. Huang, S.T. Tsai, Y.F. Huang, C.Y. Chen, J. Hazard. Mat. 140 (2007) 382–388.
[3] D. Nansheng, W. feng, L. Fan, X. Mei, Chemosphere 36 (1998) 3101–3112.
[4] G. Wang, B.B. Huang, L. Wang, Z.Y. Wang, Z.Z. Lou, X.Y. Qin, X.Y. Zhang, Y. Dai, Chem. Commun. 50 (2014) 3814–3816.
[5] R. Al-Oweini, A. Sartorel, B.S. Bassil, M. Natali, S. Berardi, F. Scandola, U. Kortz, M. Bonchio, Angew. Chem. Int. Ed. 11 (2014) 182–11185.
[6] J. Yano, V. Yachandra, Chem. Rev. 114 (2014) 4175–4205.
[7] X.F. Tang, Y.G. Li, X.M. Huang, Y.D. Xu, H.Q. Zhu, J.G. Wang, et al., Appl. Catal. B 62 (2006) 265–273.
[8] M.C. Álvarez-Galván, V.A. de la Peña O'Shea, J.L.G. Fierro, et al., Catal. Commun. 4 (2003) 223–228.
[9] X.F. Tang, X.M. Huang, J.J. Shao, J.L. Liu, Y.G. Li, et al., Chinese. J. Catal. 27 (2006) 97–99.
[10] S.L. Brock, N. Duan, S.L. Suib, J. Chem. Mater. 10 (1998) 2619–2628.
[11] J.C. Kennedy, A.K. Datye, J. Catal. 179 (1998) 375–398.
[12] S. Gupta, L. De Leon, V. Subramanian, Phys. Chem. Chem. Phys. 25 (2014) 12719–12727.
[13] T. Inturi, M. Boningari, P.G. Suidan, Environ 144 (2013) 333–342.
[14] L.Q. Ye, X.D. Liu, Q. Zhao, H.Q. Xie, L. Zan, J. Mater. Chem. A 1 (2013) 8978–8983.
[15] M. Yoshida, T. Yomogida, T. Mineo, et al., Chem. Commun. 49 (2013) 7848–7850.
[16] J.C. Nillegas, L.J. Garces, S. Gomez, J.P. Durand, S.L. Suib, Chem. Mater. 17 (2005) 1910–1918.
[17] H. Heide, R. Hemmel, C.F. Bruggen, J. Solid. State. Chem. 33 (1980) 17–25.
[18] C.L. Tang, Y.H. Huang, H. Zeng, Z.Q. Zhang, Chem. Eng. J. 244 (2014) 97–104.
[19] H.W. Zhang, J.T. Chen, P. Liang, L. Wang, J. Environ. Sci. 24 (2012) 2083–2090.
[20] Y. Tang, S.T. Martin, Geochim. Cosmochim. Acta 75 (2011) 4951–4962.
[21] Y.D. Xu, L. Yu, X.X. Guo, Appl. Catal. A 47 (1997) 164.
[22] S.C. Hou, L.T. Liu, K. Yuan, Acta Phys. Chim. Sin. 22 (2006) 1040–1042.
[23] H.W. Huang, Q. Yu, X.S. Peng, Z.Z. Ye, Chem. Commun. 47 (2011) 12831–12833.
[24] N. Kumar, R. Ramadoss, A.T. Kozakov, K.J. Sankaran, S. Dash, A.K. Tyagi, N.H. Tai, I.N. Lin, J. Phys. D: Appl. Phys. 46 (2013) 275501–275508.
[25] A. Moses Ezhil Raj, S. Grace Victoria, V. Bena Jothy, C. Ravidas, J. Wollschlager, M. Suendorf, M. Neumann, M. Jayachandran, C. Sanjeeviraja, Appl. Surf. Sci. 256 (2010) 20–29.
[26] W.X. Zhang, Z.H. Yang, Y. Liu, S.P. Tang, X.Z. Han, J. Min Chen, Cryst. Growth 263 (2003) 394–399.
[27] G. Deepa, C.K. Mahadevan, 5 (2013) 15–18.
[28] M.A. Butler, J. Appl. Phys. 48 (1977) 1914–1920.
[29] J. Zeng, H. Wang, Y.C. Zhang, M.K. Zhu, H. Yan, J. Phys. Chem. C 111 (2007) 11879–11887.
[30] R.T. Sanderson, Chemical Periodicity, Reinhold, New York, 1960.
[31] M.A. Butler, D.S. Ginley, J. Electrochem. Soc. 125 (1978) 228–232.
[32] Y. Xu, M. Schoonen, Am. Mineral. 85 (2000) 543–556.
[33] F.B. Li, X.Z. Li, Appl. Catal. A 228 (2002) 15–27.
[34] J.G. Yu, H.G. Yu, B. Cheng, X.J. Zhao, J.C. Yu, W.K. Ho, J. Phys. Chem. B 107 (2003) 13871–13879.
[35] H.F. Cheng, B.B. Huang, Y. Dai, X.Y. Qin, X.Y. Zhang, Langmuir 26 (2010) 6618–6624.
[36] J.F. Fan, et al., J. Phys. Chem. 98 (1994) 10621–10627.
[37] I.E. Wachs, J.M. Jehng, W. Ueda, J. Phys. Chem. B 109 (2005) 2275–2284.
[38] Y.Z. Li, Q. Sun, M. Kong, W.Q. Shi, J.C. Huang, J.W. Tang, X.J. Zhao, J. Phys. Chem. C 115 (2011) 14050–14057.